

Eolian controlled modification of the martian south polar layered deposits

Michelle R. Koutnik^{a,*}, Shane Byrne^b, Bruce C. Murray^c, Anthony D. Toigo^d,
Zane A. Crawford^e

^a University of Washington, Box 351310, Seattle, WA 98195, USA

^b Earth and Planetary Sciences, Massachusetts Institute of Technology, Room 54-510, Cambridge, MA 02139, USA

^c California Institute of Technology, MC 150-21, Pasadena, CA 91125, USA

^d Cornell University, 326 Space Sciences Building, Ithaca, NY 14853-6801, USA

^e University of Colorado, Boulder, LASP, UCB 392, Boulder, CO 80309, USA

Received 9 March 2004; revised 27 August 2004

Abstract

Data from the Mars Orbiter Laser Altimeter (MOLA) and Mars Orbiter Camera (MOC) aboard the Mars Global Surveyor (MGS) mission and the Thermal Emission Imaging System (THEMIS) aboard the Mars Odyssey mission have revealed unique surface features in a particular region of the South Polar Layered Deposits (SPLD). The dominant morphology is large-scale quasi-parallel grooves that extend for hundreds of kilometers with only tens of meters of vertical relief, that we have termed here the “Wire Brush” terrain. The grooves are also transected by disjointed, yet roughly continuous, low-relief sinuous ridges that cross roughly perpendicular to the trend-direction of the large-scale grooves and show only tens of meters of relief. We interpret these ridges to be eroded remnants of folded layers. At the northern end of the large-scale grooves there are non-symmetric mounds. They are frequently preceded by a significant depression and/or trailing grooves that are parallel to the Wire Brush trend. We find that a two-stage process involving winds that intermittently remove a low-density crust exposing the underlying ice to ablation is the interpretation that best explains the multitude of features observed here. These features appear to be currently inactive indicating higher winds in previous epochs.

© 2004 Elsevier Inc. All rights reserved.

Keywords: Mars, surface; Ices; Wind; Polar

1. Introduction

The MOLA and MOC aboard the MGS mission and the THEMIS aboard Mars Odyssey have revealed a multitude of features that are unique to particular regions of the SPLD. We discuss here an assemblage of unusual morphologies which occur almost exclusively in one region of the SPLD. One or more episodes of strong off-cap winds that are funneled by local topography and possibly associated with past obliquity variations and/or different SPLD and residual cap geometries leading to local surface ablation is the most plausible explanation for the unusual features we

describe here. Understanding the origin of these features is important to unraveling the overall history of the SPLD and thereby gaining insight into recent martian climatic changes (Murray et al., 2003; Thomas et al., 1992; Plaut et al., 1988; Howard et al., 1982; Howard, 2000; Cutts et al., 1976; Murray et al., 1972).

The SPLD is much younger than the Hesperian or Noachian ancient cratered terrain that underlies it (Herkenhoff and Plaut, 2000; Plaut et al., 1988). Recent analysis of the cratering record indicates a surface exposure age of approximately 30–100 myr (Koutnik et al., 2002). The polar layered deposits are believed to be composed of alternating layers of water ice with varying proportions of airborne dust and other clastics such as volcanic ash (Cutts et al., 1979; Squyres, 1979; Toon et al., 1980). Vasavada et al. (2000) found that the derived thermal inertia of the SPLD is very

* Corresponding author. Fax: +1-206-543-0489.

E-mail address: mkoutnik@u.washington.edu (M.R. Koutnik).

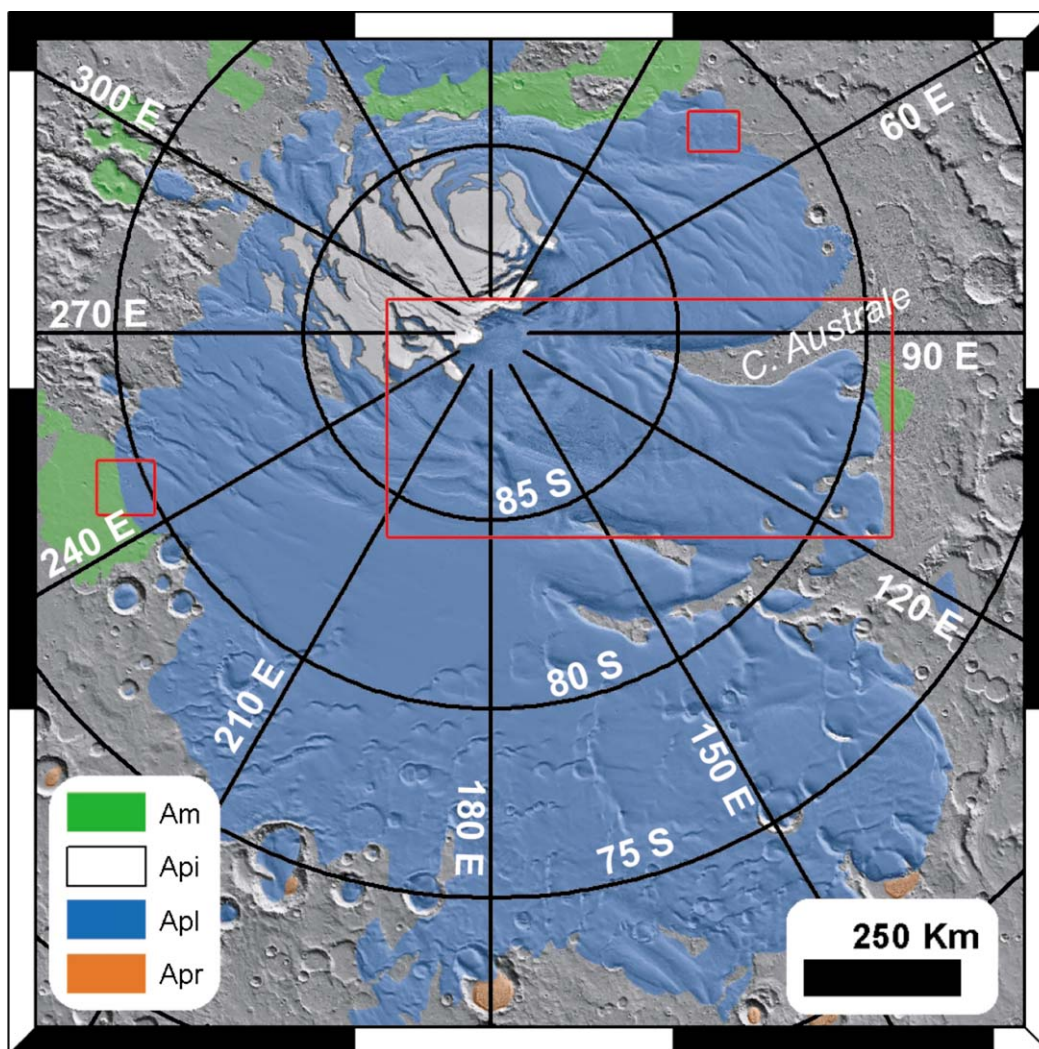


Fig. 1. MOLA shaded relief map with Amazonian geologic units in color (Kolb and Tanaka, 2001). Apl denotes polar layered deposits; Api denotes polar ices (residual CO_2); Am denotes mantle; Apr denotes sand deposit. The large red box denotes the location of our primary study area, which is the full extent of Fig. 2. The other two red boxed areas at the margins highlight other areas of similar grooved terrain.

low ($50\text{--}100 \text{ J m}^{-2} \text{ s}^{-1/2} \text{ K}^{-1}$), suggesting that the uppermost few centimeters of the SPLD surface is composed of very low density material, free of a significant amount of rock or ice. Hofstadter and Murray (1990) independently argued that the stability of sunward-facing SPLD scarps at high southern latitudes likewise requires an insulating ablation crust that is resistant to current wind scouring. Areas where this mantling deposit is inferred to be only millimeters thick have recently been discovered (Titus et al., 2003). In contrast the average thermal inertia of the North Polar Layered Deposits (NPLD) was found to be much higher, $450\text{--}600 \text{ J m}^{-2} \text{ s}^{-1/2} \text{ K}^{-1}$ (Vasavada et al., 2000), indicating that water ice is likely the dominant material at the surface in this location and that any insulating crust must be much thinner than in the south or not present at all. Unlike the SPLD, most of the NPLD is covered by the permanent water ice residual cap which may be even the site of current ice deposition (Mischna et al., 2003). We suspect that the presence of this unusual low-density surface crust of some centime-

ters thickness only on the SPLD may be an important link in the erosional process which produced the Wire Brush terrain, and would also explain why this terrain is absent from the north polar deposits where this crust is much thinner or not present.

The region of study is confined to $80^\circ\text{--}265^\circ \text{ E}$, $80^\circ\text{--}87^\circ \text{ S}$, with a primary focus $80^\circ\text{--}180^\circ \text{ E}$, $80^\circ\text{--}87^\circ \text{ S}$ highlighted in Fig. 1. The MGS spacecraft ground track is tangent to 87° S latitude so there is dense data coverage in the majority of our study area. Unfortunately, there are virtually no data from $87^\circ\text{--}90^\circ \text{ S}$, an important region for this work that we are unable to view with the MGS data. For this region we utilized the Viking images there that have been processed into the Mars Digital Imaging Map (MDIM) 2.1 (produced by the USGS).

The primary data sets used for this work are the shaded relief maps, slope maps and topography profiles derived from the 115 m pixel^{-1} resolution MOLA Digital Elevation Map (DEM) (Neumann et al., 2001), MOC-NA images up though

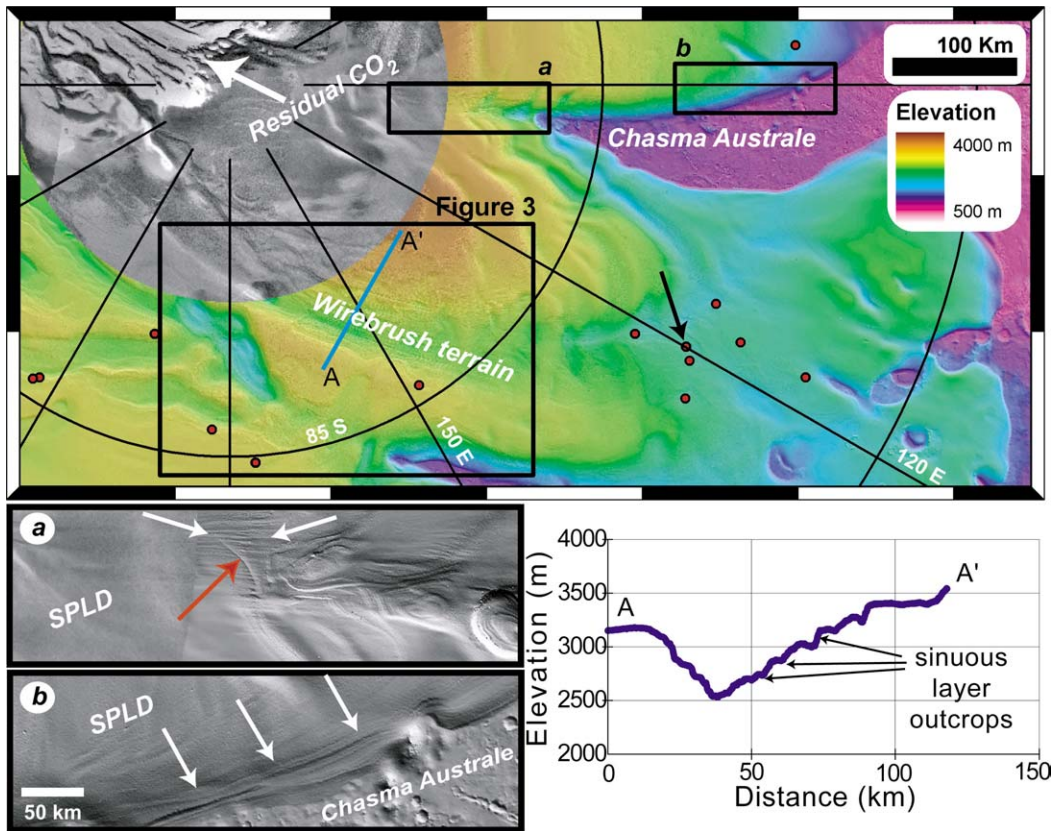


Fig. 2. Topography of the study area with shading provided by MOLA and Viking MDIM 2.1 (poleward of 87° S). The boxed regions highlight locations of Wire Brush terrain. The regional depression containing the primary region of Wire Brush terrain (Fig. 3) can be seen in the topographic profile shown (AA'). The insets show the grooves visible at the head and along the western wall of Chasma Australe. Red points show the locations of mounds within this area. Topography of the mound indicated by arrow is shown in Fig. 5. White arrows in sub-panel (a) and (b) show the distinctive ‘wirebrush’ grooving. Red arrow in sub-panel a shows an example of a cross-cutting ridge which are common in this region (snake features; see Fig. 3).

extended mission phase R02 (February 2003), and the released THEMIS images. The shaded relief maps provide the most advantageous view of large-scale surface features that are difficult to recognize in visible imagery (see Figs. 1, 2, and 3). This exquisite rendering of low relief terrain arises from the exceptionally high vertical precision of the MOLA instrument (better than 1 m vertically), the filtering of overlapping sampling in the MOLA data, and the absence of atmospheric and undesirable illumination effects to obscure the subtle topographic relief of these SPLD features as described by Neumann et al. (2001).

2. Descriptions of unusual features

2.1. Regional description

The study area for this work is a portion of the unit considered polar layered deposits, Apl, as mapped by Kolb and Tanaka (2001). Figure 1 shows the entire SPLD (Kolb and Tanaka, 2001) with the residual cap outline shaded white. Our primary study area, 80° – 180° E, 80° – 87° S, is highlighted in Fig. 1 and shown in Fig. 2. Chasma Australe is located in the west of this area and there are enclosed chas-

mae features in the east and north–east of the primary study area.

The most notable feature of the study area is large-scale grooving that cuts into the SPLD, that we term here “Wire Brush” terrain, and which was first recognized in Viking imagery by Howard et al. (1982) (see their Fig. 16). This terrain is found dominantly in this region and also at the head of Chasma Australe (see insets in Fig. 2). There are only two other small regions on the SPLD that appear to have more localized versions of this grooving and they are shown as red boxes on Fig. 1. No regions of the NPLD exhibit this morphology. At the distal (northern) end of the main region of Wire Brush terrain is a clustering of mounds shown by red dots in Fig. 2 (roughly 120° E, 83° S) that have trailing grooves trending in the direction of the Wire Brush grooved terrain (see Fig. 5 and later discussion).

Figure 2 shows a zoom-in view of the Wire Brush terrain and also the association with the current position of the residual cap as evident in Viking data. This region also contains curvilinear ridges, which we term here “snakes,” that are uniquely exposed in areas containing Wire Brush terrain. The snakes are irregular in strike but trend roughly perpendicular to the grooves.

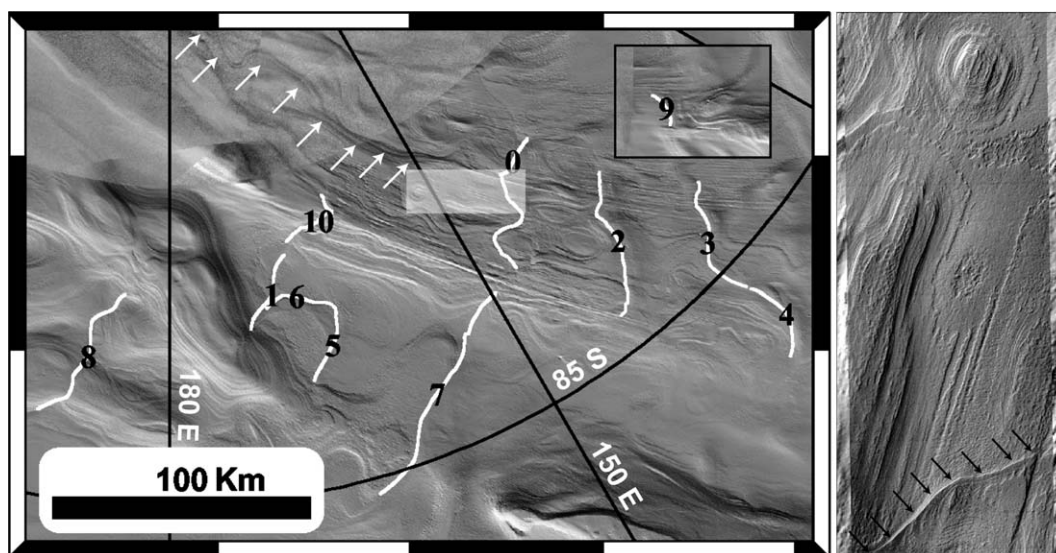


Fig. 3. Eleven snake features in the wirebrush region and head of Chasma Australe (inset) are identified by white lines. Numbers correspond to snake ID in Table 1. Inset in top right shows another example of a snake above the head of Chasma Australe and is centered on 87° S, 90° E at the same scale as the main image. Background is provided by MOLA shaded relief and USGS produced Viking MDIM 2.1 poleward of 87° S. The light-shaded rectangle indicates the position of the right panel (rotated), which shows an individual snake (dark arrows) distinctly (THEMIS VIS frame V08692011). This THEMIS frame also shows examples of the surface grooving which characterizes this wirebrush terrain and a distinct circular feature at the top of the frame indicating unusual erosion. Additionally, distinct erosional north–south forms, caused by individual resistant layers cropping out, also occur in the wirebrush area, an example of which is illustrated by white arrows.

There are also sinuous forms (see example indicated by arrows in Fig. 3) roughly aligned in a north–south direction (sometimes leading to circular and oblate features). They can be traced back to a scarp in the current residual CO_2 cap with the Viking MDIM. These sinuous forms are likely to be individual resistant layers originally exposed in the steep scarp within the residual cap, and now are widely separated in plan view due to the much lower slope in this regional depression.

2.2. Wire Brush terrain

The details of the Wire Brush terrain are best expressed in the MOLA topographic shaded relief map as shown first by Neumann et al. (2001). A close-up of the primary study area is shown with MOLA and Viking data in Fig. 2. We have recognized this grooved pattern only here, in small areas at the tip and on the wall of Chasma Australe, and possibly small regions at the eastern edge of the SPLD at 255° – 260° E, 79° S and at 35° – 50° E, 82° S. These regions are shown as boxed areas on Fig. 1. We have not found examples of this terrain on the NPLD.

The primary area of Wire Brush terrain is located in a subtle, regional-scale depression within the SPLD, as evident from the topographic profile in Fig. 2. This area has been mapped in detail by Kolb and Tanaka (2003). The depression has a sloping side on its eastern edge, leading down toward the trough floor and then nearly flattens out (but slopes slightly uphill) toward the west. The trough existed prior to the formation of the Wire Brush grooves seen today. We will later argue that this trough was a necessary

prerequisite for groove formation. The relief on the discernable wall (to the east) is about 600 m at the location shown in the topographic profile in Fig. 2. The width of the depression is approximately 80 km and the maximum extent of the Wire Brush terrain is approximately 400 km. In isolated cases individual grooves appear continuous over this entire distance, but generally the grooves are visibly continuous for only 40–100 km. The vertical relief of the grooves is about 10–50 m. Individually they range in width from 600–1400 m. The strike of the grooves appears to curve to the left (west) as one moves equatorward; consistent with Coriolis deflection of northward flowing material (i.e., wind).

The grooves at the tip of Chasma Australe and along the exposed wall, shown in Fig. 2, can be seen in the MOLA data to extend for at least 80 km (they extend for an unknown distant poleward of 87° S).

This ridge-groove topography resembles yardangs or mesoscale eolian streaks (Thomas et al., 2003). Yardangs (isolated elongated ridges) are formed through abrasion by saltating material which is currently absent on the SPLD. The mesoscale linear streaks reported by Thomas et al. (2003) have a similar appearance in plan view but, in contrast to these polar features, have no appreciable topographic relief.

2.3. Snakes

Spaced throughout the Wire Brush region are curving ridges we have termed snakes (to avoid genetic implications). Their positions across the Wire Brush terrain are indi-

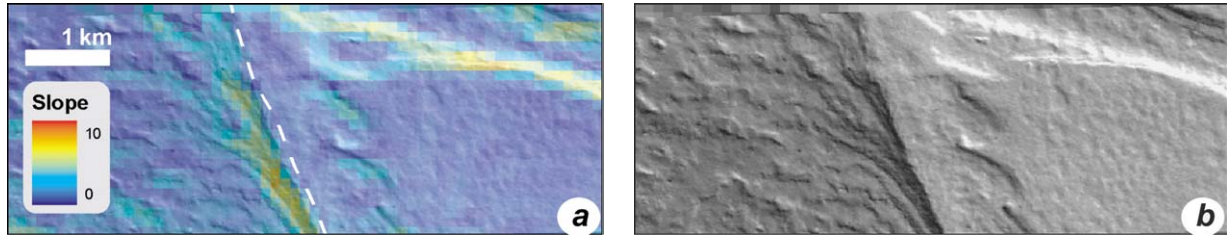


Fig. 4. Example of mapping methods for snake features. Slope data (in degrees) can be overlaid on higher resolution MOC images as shown in (a) which eases the mapping process. The dashed white line indicates the mapped location of the crest of the sinuous ridge. The color scale saturates at 3° to better show slopes on the shallow side of the snake. The MOC background to the slope data (image M03/04509) is shown in (b) for clarity. Location is 86.4° S, 142.2° E, illumination from the upper right.

cated on Fig. 3. These ridges are generally asymmetric with layering exposed on the steep but not the shallow side. Their relief is minor and is typically only tens of meters. The examples shown in Fig. 3 are the most prominent and can be up hundreds of kilometers in length. This combination of characteristics hypothetically could be due to (1) thrust or normal faulting within the ice sheet with each observed snake being a trace, or (2) erosional remnants of contorted layers. Layering is commonly exposed within the snakes, ruling out a surficial origin.

To investigate the possibility that the snakes are traces of low-angle faults we test whether the three dimensional locations of points on these putative surface traces can be approximated by a single plane. We have mapped their surface expression using a combination of shaded relief and slope maps from MOLA and visible imagery from MOC and THEMIS. Slope-maps show the snake crest well due to their asymmetrical nature. Figure 4 shows an example of this mapping. In some locations where the surface trace was uncertain we did not continue mapping the feature (such as westward of feature 0). Once these features have been mapped out in this manner we can easily extract the elevation and position of each point. The elevation is calculated from the 115 m pixel^{-1} DEM using bilinear interpolation of the surrounding four pixels. The x and y location is given as meters in a polar stereographic projection with (0, 0) being at the South Pole (positive y axis along zero longitude). The result of this analysis is a set of measurements of the trace of each individual snake in three dimensions. We investigate these traces by attempting to fit planes to these measurements using linear regression. To determine how accurately each snake can be represented by a single plane we examine the residuals between this plane and the original data points. The mean of these residuals is of course zero as this is a best fit to the data; however, the magnitude of their standard deviations can indicate the quality of the fit plane as a descriptor of these data.

We summarize the results of this analysis for each snake, or in some cases combinations of snakes (where we believe different sections belong to the same feature), in Table 1. An inclined plane fit has only three free parameters. It can be seen from the second column in Table 1 that each fit has more than sufficient data points to constrain the final solu-

Table 1
Information on planar fits to snake data

Snake ID	No. of points	σ of data	σ of residuals	Slope of plane ($^\circ$)
0	509	182.55	20.53	0.74
1	254	112.02	39.76	2.10
2	496	158.52	87.25	0.62
3	408	122.27	39.74	0.69
4	270	69.28	8.30	1.15
3 & 4	678	132.23	83.41	0.44
5	256	50.18	5.33	0.33
6	224	19.42	5.66	0.65
5 & 6	480	62.56	9.38	0.36
7	703	146.67	79.71	0.96
8	486	91.19	58.12	1.83
9	109	46.19	5.84	0.67
10	227	171.95	10.41	2.01

The snake ID corresponds to lines on Fig. 3. In all cases the standard deviation of the residuals is substantially less than that of the data itself; however in many cases it is still high enough to make a plane a bad approximation of these features. The extremely shallow dips of these planes cast doubt on the fault scarp interpretation discussed in the text.

tion. The standard deviation of the residuals, which we use as our quality indicator, can thus be considered to be a reliable commentary on the validity of approximating these features as fault planes. The standard deviation of the elevation data for each snake is also given for comparison and can be interpreted as the residuals that would result from a best fit horizontal plane to the data. In all cases a significant improvement in the magnitude of the residuals was noted when moving to a fit using an inclined plane.

Several snake features such as 4, 5, 6, 9, and 10 show an excellent agreement with this inclined planar fit. Residuals of some of the other snake features, e.g., 1, 2, 3, 7, and 8 are so large that even an inclined plane is a very poor descriptor of those data. However, also shown in Table 1 is the dip for each fit plane. As can be qualitatively inferred from their sinuous nature in plan view these dips are extremely low. The extremely low nature of the inferred dips of any such “faults” calls into question their physical realism. Such low angle faulting is extremely rare in natural geological systems and the mechanisms by which it would be generated here are unclear. Hence, below we propose another explanation of the origin of these peculiar features which are observed only in the Wire Brush region.

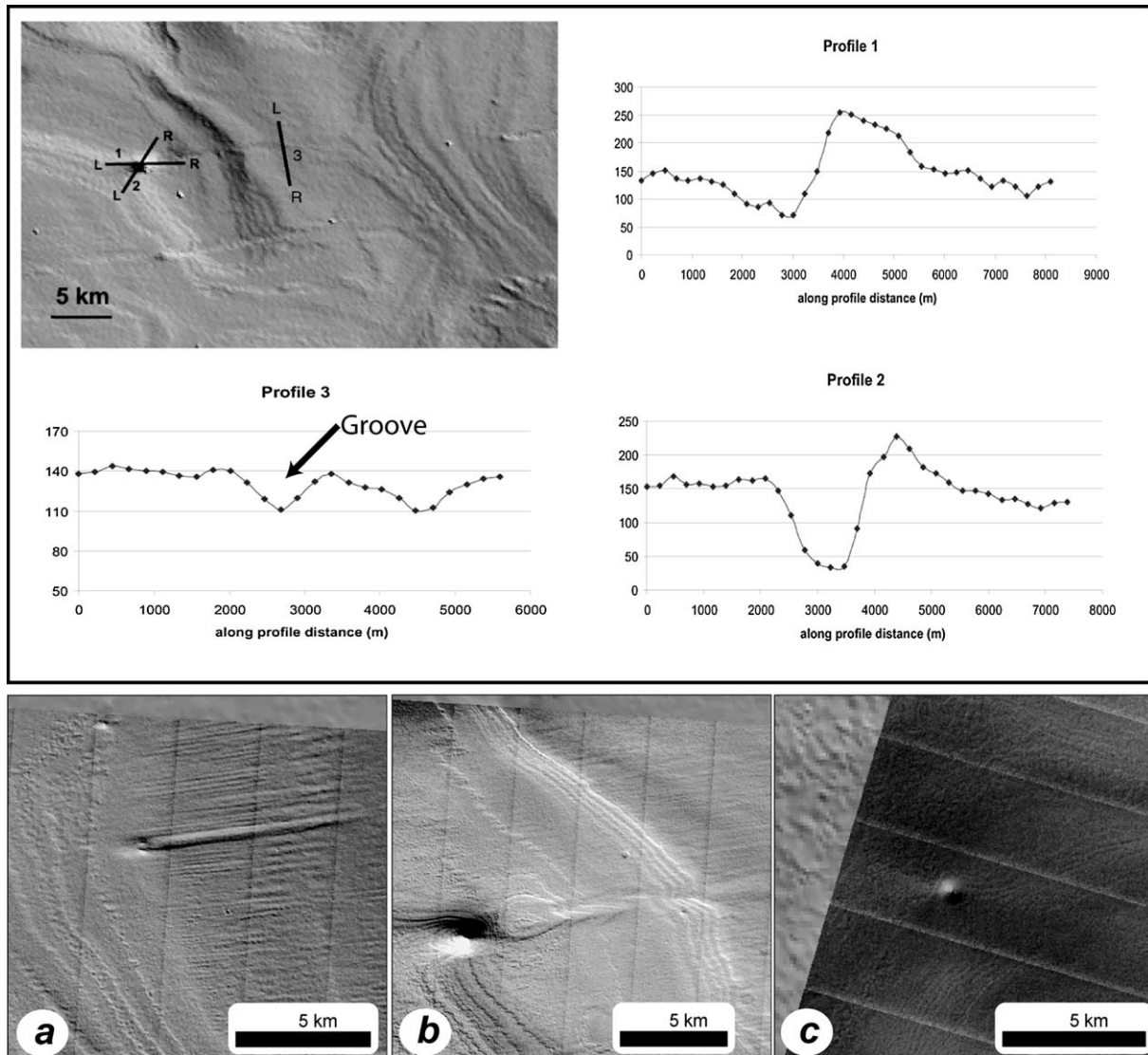


Fig. 5. MOLA shaded relief map view of some of the mounds with trailing grooves. Profiles 1, 2, and 3 are oriented from left (L) to right (R) and their locations are shown in the context panel. Profiles 1 and 2 show the characteristic shape of a mound in this region, illustrated with an arrow in Fig. 2. This often includes a leading depression and/or a trailing groove, part of which is shown in Profile 3. Sub-panels (a), (b), and (c) show examples within the THEMIS VIS dataset of SPLD mounds. Panels (a) and (b) are within the wirebrush region (both from V08879005, illuminated from lower left) and show trailing grooves. Panel (c) is located outside the wirebrush region (at 85.5° S, 240° E, V08526009, illuminated from upper left) and shows a comparable mound with no trailing or leading depressions.

2.4. Mounds with trailing grooves

There are at least nine distinct, non-symmetric mounds within the primary region of Wire Brush terrain. However, mound structures are not unique to this region of the SPLD. Figure 2 shows the distribution of the most prominent mounds in the full extent of our study area. Key defining characteristics of each of the nine mounds are shown in Table 2. They all have the same general shape and range from 820–2750 m in diameter and from 30–160 m in height. All mounds in the study area exhibit a leading depression, located on the south-facing side (poleward), just before the positive relief of the mound begins. The depth of the depression ranges from 20–120 m. Toward the northern end

of the primary region of Wire Brush terrain there is a clustering of mounds, most of which have trailing grooves that trend along the direction of the Wire Brush grooves. Adjacent mounds, outside the approximate bounds of the east–west coverage of the Wire Brush terrain, do not have trailing grooves. There are also a few mounds amongst the large-scale grooves that do not exhibit trailing grooves.

Topographic profiles over one of the mounds are displayed in Fig. 5. They show that it is non-symmetric and has a preceding depression on the south-facing (poleward) side. This structure is characteristic of all mounds in the study area. A section across the trailing groove is shown in Fig. 5. The trailing grooves are close to the resolution limit of the MOLA DEM so their shape and width cannot be well deter-

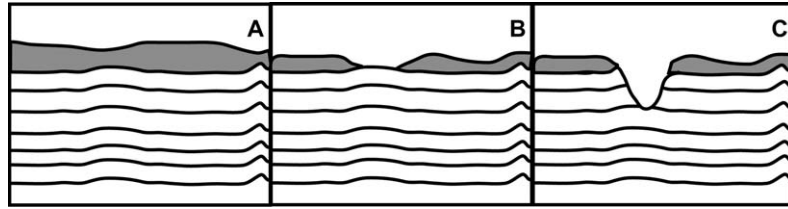


Fig. 6. Two-stage formation mechanism for the Wire Brush terrain shown in cross-sectional view. A is the initial surface, B results from off-cap winds funneled locally across the surface, and C results from the subsequent ablation of the exposed ice. A sublimation lag is expected to re-accumulate over the bare ice in response to ablation which provides a natural mechanism to end this groove-formation process. See text for discussion. Not to scale.

Table 2

Characteristics of non-symmetric mounds in the Wire Brush region

Mound ID	Diameter (m)	Maximum relief (m)	Minimum relief (m)	Trailing groove	Size of depression on south-facing side (m)
1	820	140	80	no	40 to 80
2	950	60	40	no	60
3	960	60	30	yes	40
4	1200	100	55	no ^a	80
5	1250	100	60	no ^a	70
6	1475	60	30	yes	20
7	2500	120	50	no ^a	85
8	2600	160	40	no	40 to 120
9	2750	100	40	yes	100

Note. Some mound characteristics are summarized here. The relief of these features depends on the direction over which the topographic profile is taken (due to variations in the level of the surrounding terrain); both maximum and minimum values are given here.

^a The mound is outside the primary region of Wire Brush terrain.

mined. THEMIS VIS data illustrate the visible appearance of these mounds and their associated grooves, two examples are shown in Figs. 5a and 5b. Figure 5c shows an example of a mound outside the wirebrush area, it is similar in size but has no associated groove. Although there are mounds like these scattered throughout the SPLD, only mounds within the wirebrush region show trailing grooves.

3. Unified explanation

In the past we have considered a number of formation mechanisms for the features discussed above (Crawford et al., 2002; Koutnik et al., 2003). Initially we considered not only wind erosion but also volcanic and glacial flow processes as possible mechanisms. Explanations requiring volcanism and glacial flow are more elaborate than wind alone and are less plausible. The basic theory we now propose is that the shape and direction of these features is controlled by the wind. Aeolian action can strip the surface mantling layer exposing the underlying ice of the layered deposits. Insolation-driven sublimation can then excavate these features. Although wind controls the location and orientation of the features it is the Sun that actually forms them. We favor this unifying two-stage wind-driven explanation and abandon our other earlier speculations on the formation of these features at this point.

3.1. Wire Brush terrain

In order for this method to produce grooves extending for hundreds of kilometers that are meters deep there are at least two requirements. Firstly, a regional topography favorable for large-scale channeling of off-cap winds must have already existed. This will serve to channel the wind and create a region of higher wind velocities and surface wind stress compared to surrounding areas of SPLD. This requirement is consistent with the primary observed locations of Wire Brush terrain in a large trough and at the head of Chasma Australe. Secondly, there must be a low-density crust that is easily erodable compared to the underlying ice-rich deposit. This surface crust gets scoured locally where the channelized wind is greatest, exposing the underlying ice-rich SPLD. After this point the propagation of the groove is primarily controlled by ablation of the underlying ice. We infer it would be self-sustaining provided there are continued episodes of high winds. A cartoon of this process is shown in Fig. 6. This mechanism explains why the Wire Brush terrain is found dominantly in the two large-scale outward facing troughs on the SPLD where strong wind channeling is plausible. It can also explain the downslope extent of the groove structures in the primary area. They have a natural end where the trough widens sufficiently so it can no longer serve to funnel the wind. The requirement of the erodable crust overlying ice-rich material could explain why this Wire Brush terrain is unique to the SPLD. The lack of an overlying crust on the north polar layered deposits prevents the formation of Wire Brush terrain at the head of Chasma Boreale or other north polar trough sites. The strong temperature contrast provided by the nearby residual CO₂ ice also helps generate strong winds. It is possible that the outward facing troughs found to the northeast of the main wirebrush region lack this scouring because they are further from the residual CO₂ and thus have lower wind speeds in general.

Model runs using a Mars mesoscale model (Toigo and Richardson, 2002) were performed in order to investigate the wind stress values near the Wire Brush terrain and Chasma Australe. Model runs were performed at $L_s = 255$ (late southern spring) when wind stresses are expected to be at their highest. Three other model runs were performed at $L_s = 75, 165,$ and 345 (evenly spaced throughout the year). Wind velocity in any one area varies throughout the year as the seasonal frost cap changes size. Competing effects de-

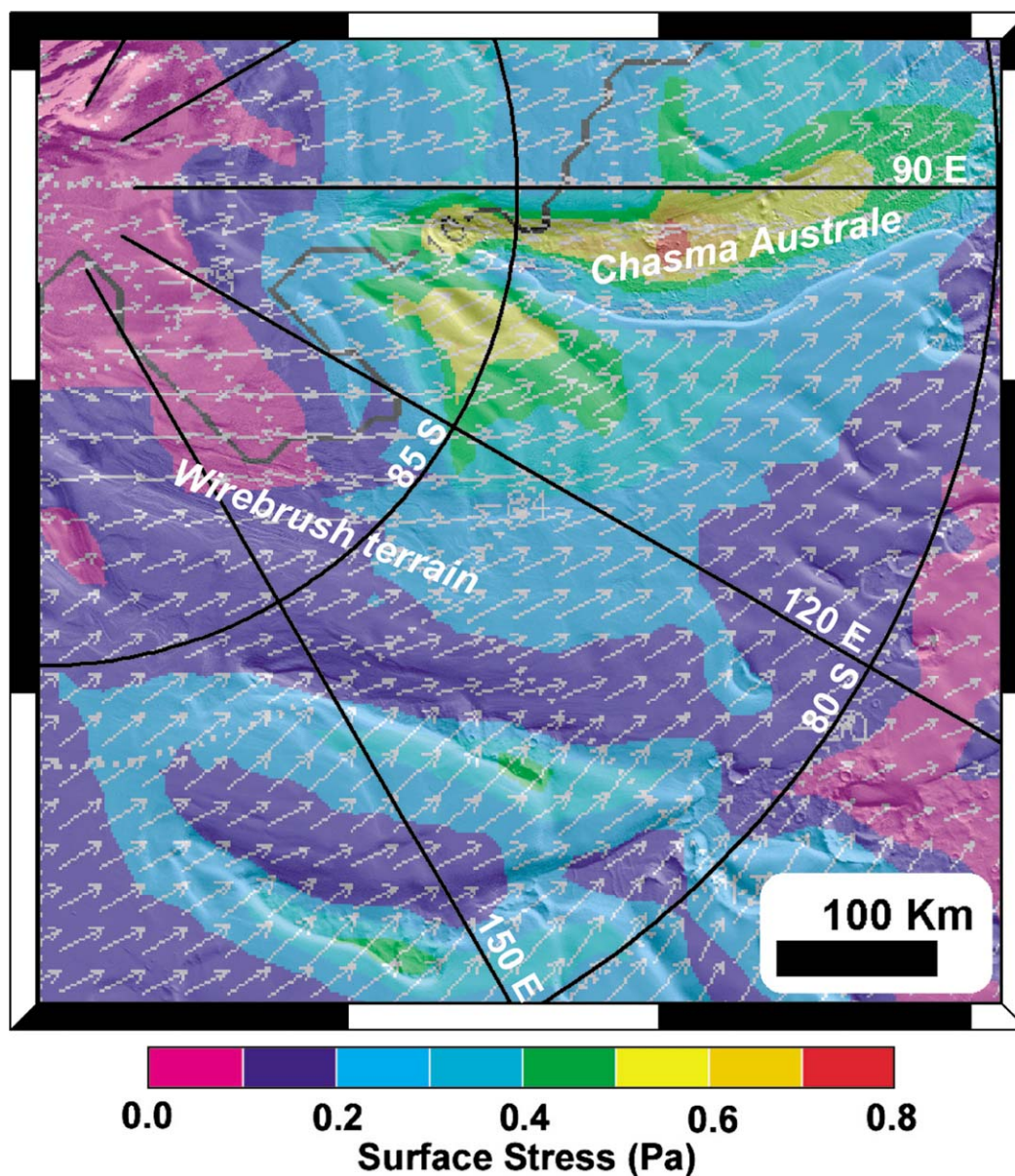


Fig. 7. Mesoscale model results showing wind stress values for the current SPLD topography and residual cap geometry at $L_s = 255$ (late southern spring) and local time of 6 pm at Chasma Australe. Winds are highest in Chasma Australe during the evening. Arrow direction represents wind direction and length shows wind speed.

scribed in detail by Toigo et al. (2002) exist which result in $L_s = 255$ being favored above others for wind production. The model runs we performed at other seasons confirm this season has the highest wind stresses in these locations. Our simulation results were outputted every hour for a 24 period to determine the local time of highest wind conditions (displayed in Fig. 7). The model uses topography from MOLA and the current south residual cap configuration. Wind stress values range from 0.00 to 0.08 Pa in this simulation. It has been determined from wind tunnel tests that a value of 0.04 Pa or above is sufficient to mobilize the most easily moved (sand sized) particles, which may be an indication of when crust erosion can be initiated. The global domain (60 km surface cell-size) runs indicates that winds are high near the cap

edge, generating a high wind stress, and occur primarily at local noon and late evening. The local domain (12 km surface cell size) also indicates the highest wind velocities and wind stress at the cap edge also in the late evening. Figure 7 shows that the highest wind stress of the entire local domain is 0.08, reached in Chasma Australe. The high winds evident in Chasma Australe do confirm the extent to which winds are being funneled by this large trough. Significantly we see Wire Brush terrain at the poleward tip of Chasma Australe and on its western wall (see Fig. 2) which correlates with high wind stress values there predicted by the model. This correlation supports our hypothesis that the surface grooves of the Wire Brush terrain have been formed by wind. The fact that the model outputs do not show exceptionally high

wind stress in the primary region of Wire Brush terrain may suggest that the primary region of Wire Brush terrain formed under a previous obliquity/climate epoch. The position and size of the residual cap has varied in previous times and may have provided a greater thermal contrast near the wirebrush area increasing the wind speeds. Other nearby depressions (chasmae) also show relatively high wind stress values and also may show faint Wire Brush type terrain. These model results show both that topography does effectively increase wind speeds and that the wind directions (arrows in Fig. 7) align with the current wirebrush grooves.

Usually, sand-sized particles are required to erode a surface through eolian action. There is currently very little sand on the surface of the SPLD and it difficult to imagine how significant quantities of sand could have been supplied to these locations in previous epochs. Dust aggregates, on the other hand, have been suggested to comprise the sand sized particles that currently surround the NPLD (Greeley, 1979; Saunders and Blewett, 1987). Perhaps a similar process has been possible during the history of the SPLD. In addition, sand sized particles may not be required to initiate these grooves. Shallow erosion of the SPLD by venting of CO₂ gas and dust from beneath the seasonal frost has recently been documented (Kieffer, 2000; Piqueux et al., 2003). Hence, we think it is plausible that adequate amounts of eroding clastic particles have been available from time-to-time to facilitate the efficient two-stage erosional process we hypothesize.

3.2. Snakes

The sinuous east–west ridges we have termed snakes are only seen in areas that have wirebrush grooving. It is reasonable to assume therefore that either their formation or exposure is connected with processes that only operate in these regions. We have already demonstrated the implausibility that the snakes are either surficial deposits or low-angle fault traces. A more attractive possibility we have considered is that these features are surface erosional modifications of compressed and distorted layers within the ice sheet. The asymmetric shape of the snake with layering exposed only on the upwind side is likely due to sustained wind erosion of the protective mantling deposit and subsequent ablation. Figure 8a diagrams this process and shows the inferred region of eolian erosion. Possible explanations of this folding include sub-SPLD tectonics or (less-likely) flow of SPLD material over irregular basal topography. We do know that these features penetrate deeply into the SPLD. Figure 9 shows a snake feature intersecting a 1 km deep chasma. The superposed elevation contours show the shape of the scarp is affected (it is steeper at the snake location) over this entire depth range (2100–3200 m elevation).

Are such compressional distortions within the SPLD restricted to the Wire Brush terrain? We think not, rather they are only exposed in those areas because only there do unusually high and sustained off cap winds erode through the crust and expose underlying ice to ablation.

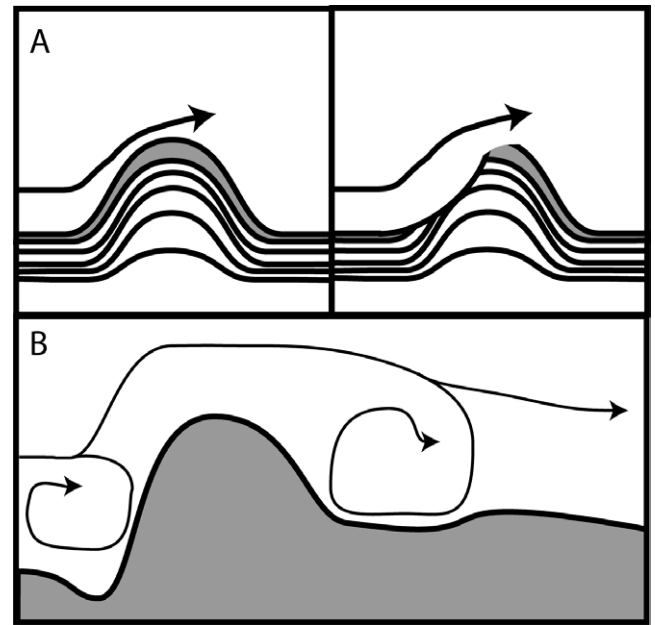


Fig. 8. (a) Cartoon showing formation mechanism for the snake features. (b) Cartoon showing formation mechanism for the leading depression and trailing groove associated with the mounds. See text for discussion. Not to scale.

3.2.1. Mounds with trailing grooves

Mounds present obstructions to the wind being funneled through this area. Turbulent affects from the wind/mound interaction could remove the protective mantle material on the south-facing side of the mound, contributing to the leading (polar-facing) depression. Similar turbulent effects could also remove material downwind from the backside of the mound, resulting in a trailing groove, propagated by an ablation mechanism, similar to that we propose for the grooves in the Wire Brush terrain. Figure 8b illustrates this conceptual mechanism. The only mounds with trailing grooves are near to the Wire Brush terrain and directly in line with the trend of the grooves, though this is not the case for every mound in this path. Although, close to the resolution of the MOLA DEM the trailing grooves appear to be almost uniform in width extending out from the mounds. The mounds without trailing grooves are primarily found near the margins of the east–west extent of the Wire Brush terrain, where there are also no large wirebrush grooves, supporting the interpretation that the trailing grooves are associated with winds funneled through this regional depression. It is also important to note that there are many other mounds found elsewhere across the SPLD, none of which have trailing grooves, e.g., Fig. 5c.

4. Discussion and conclusions

4.1. Timing of events

Deducing the timing of events is often difficult from orbital data alone. Some timing information can come from

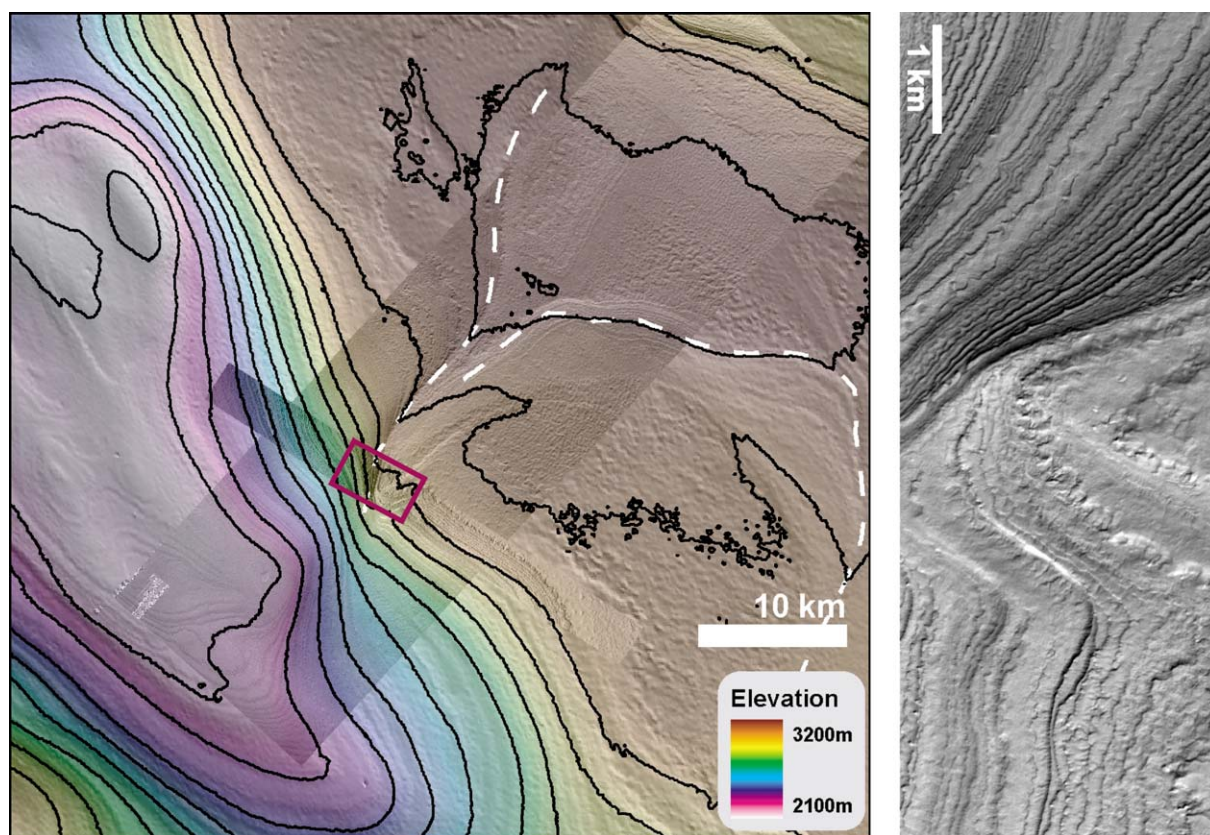


Fig. 9. Intersection of snake 1 (see Fig. 3) with a 1 km deep closed chasma within the SPLD. The white dashed lines illustrate the trace of the snake features 1 and 5 (see Fig. 3) which can be seen in the underlying THEMIS VIS image (V08781005). The MOLA topography (with contours plotted every 100 m) shows a steepening of the scarp associated with the snake. This demonstrates that the snake is a 3D structure with significant (at least 1 km) relief. The red box in the left panel outlines a section of the MOC image (E11/03053) in the right panel (rotated 45° clockwise, illuminated from the lower left). The layering wraps around the bulge in the scarp with no evidence of any faulting.

examining the impact crater population within this region. There is a population of eight small craters ranging from 165 to 650 m in diameter within the primary region of Wire Brush terrain, as shown in Fig. 10. The two smallest craters appear to be fresh, based on their bowl-shape and maintained rim. The abundances, sizes and morphologies of these impact craters are not significantly different from those recognized generally over the South Polar Layered Deposits (Murray et al., 2003; Koutnik et al., 2002). This implies that the broad outline of SPLD history that has been inferred previously probably applies to the Wire Brush region as well. It may have been the formation of the grooving itself which was responsible for the resurfacing; however, the dearth of small craters is characteristic of the SPLD as a whole while the wirebrush grooves are restricted to this area so we do not consider this possibility to be likely.

Koutnik et al. (2002) argued for a resurfacing of the SPLD within the last few 10^5 years based on the relationship between the populations of craters of this size and those of greater than 1 km in diameter. If this resurfacing event acted in this region then most craters smaller than 250–300 m were removed within the last 10^5 to 10^6 years. Such resurfacing may have resulted from 30–40 m of uniform blanketing of

new ice, or by removal of a comparable amount through uniform erosion (Schaller et al., 2003). The Wire Brush features manifested in this region certainly would have been modified by such an episode, but not obliterated. Hence, the general outline and character of the features may predate that episode.

Is the Wire Brush terrain sculpting process currently active? One objection to current activity is that the observed fresh to moderately-fresh impact craters provide similar obstacles to flow as do the mounds with trailing grooves. However, there are no trailing grooves or other unusual erosional attributes associated with these craters.

We envision the ablation mechanism to shut off naturally as an ablating icy surface will form a sublimation lag of non-volatile material. When eolian action cannot remove this lag the formation of grooves ceases but may be reactivated during a subsequent high-wind period. The lack of any thermal anomaly (within examined THEMIS IR frames) associated with the floors or the tips of these grooves indicates that they are not currently forming; however, this does not constrain the age of the features.

Finally, the wind flow simulations of Fig. 7 do not indicate that the Wire Brush region is currently the site of maximum wind stress, in contrast to Chasma Australe, for

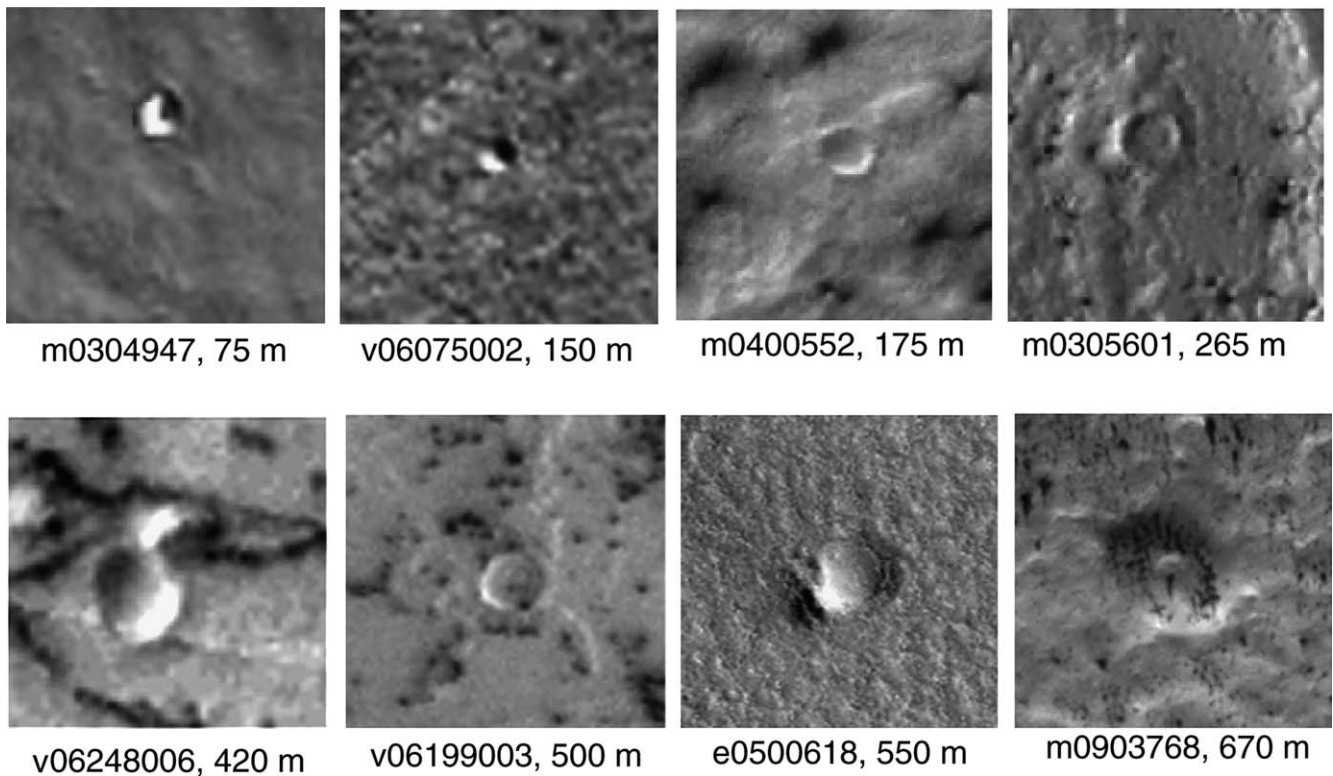


Fig. 10. Impact craters found within the region of Wire Brush terrain. The craters are seen in MOC NA and THEMIS images. They are all shown at different scales but their diameters are given. The craters generally show significant modification but lack the directional eolian erosion of other features in this region.

example. Our simulations span a full range of L_s and this result is consistent across all these model runs. In our view, the Wire Brush features date back to a period of higher off cap winds when higher wind stresses in the Wire Brush region were more favored, perhaps associated with some previous obliquity or differing position of the residual cap preceding the resurfacing episode of 10^5 – 10^6 years ago.

4.2. Topographic implications

Topographic channeling of regional winds appears to be a key characteristic of groove formation. We conclude that the current topographic setting of the Wire Brush terrain is an essential component of its history, and must have persisted since before the time that Wire Brush terrain formed. The simulated high wind stress values in Chasma Australe (Fig. 7) correspond even to where grooves are seen on the walls in Fig. 2.

Chasmae are common in this region of the SPLD, including closed depressions like that immediately east of the Wire Brush terrain. Their channeling effect is similar to Chasma Australe in providing an efficient pathway to accelerate off-cap winds. Intense wind stripping of the residual crust enabling subsequent ablation may have played an important role in sculpting all of these features, not just in the immediate Wire Brush region.

We do not speculate here how the observed mounds, acting as protruding obstacles, were formed nor of what they

are composed. It is only necessary to our hypotheses that they existed before the Wire Brush terrain formed. Wind stripping provides a plausible explanation for the trailing grooves that are found downwind from the mounds and for their upwind depressions. Similarly intense wind stripping and erosion of transecting compressional ridges in the Wire Brush region explains why these snakes are only exposed in the Wire Brush area, even though they may well be common throughout the SPLD.

4.3. Conclusions

We find that episodes of topographically channeled high winds which remove a low-density crust and expose underlying ice to ablation, may explain the assemblage of unusual morphological features evident in the wire brush region, 80 – 180° E, 80° – 87° S. This interpretation is consistent with the absence of Wire Brush terrain on the NPLD, where a conspicuous low-density crust is not found. In particular, the large-scale grooves, the snakes, and the trailing grooves downwind from isolated mounds within the Wire Brush region can also be explained by this two-stage erosion process. Erosion and sculpting of the neighboring chasmae may also reflect these circumstances. The last episode of unusually high winds probably took place before the major resurfacing episode 10^5 – 10^6 (Koutnik et al., 2002) years ago implied by the small-crater population.

Acknowledgments

We thank Oz Pathare (Caltech), Bernard Hallet (University of Washington), Eric Kolb (University of Arizona), and Ken Tanaka (USGS) for their contributions and useful discussions. We are grateful to Lori Fenton and an anonymous reviewer for detailed constructive reviews that greatly improved this manuscript.

References

- Crawford, Z., Murray, B., Byrne, S., Koutnik, M., 2002. Surface features of the south polar layered deposits. In: American Geophysical Union Fall Meeting 2002.
- Cutts, J.A., Blasius, K.R., Briggs, G.A., Carr, M.H., Greeley, R., Marsursky, H., 1976. North polar region of Mars: imaging results from Viking 2. *Science* 194, 1329–1337.
- Cutts, J.A., Blasius, K.R., Robert, W.J., 1979. Evolution of martian polar landscapes: interplay of long-term variations in perennial ice cover and dust storm intensity. *J. Geophys. Res.* 84, 2975–2994.
- Greeley, R., 1979. Silt-clay aggregates on Mars. *J. Geophys. Res.* 84, 6248–6254.
- Herkenhoff, K.E., Plaut, J.J., 2000. Surface ages and resurfacing rates of the polar layered deposits of Mars. *Icarus* 144, 243–253.
- Hofstadter, M.D., Murray, B., 1990. Ice sublimation and rheology—implications for the martian polar layered deposits. *Icarus* 84, 352–361.
- Howard, A.D., 2000. The role of eolian processes in forming surface features of the martian polar layered deposits. *Icarus* 144, 267–288.
- Howard, A.D., Cutts, J.A., Blasius, K.R., 1982. Stratigraphic relationships within martian polar cap deposits. *Icarus* 50, 161–215.
- Kieffer, H.H., 2000. Annual punctuated CO₂ slab-ice and jets on Mars. In: 2nd International Conference on Mars Polar Science and Exploration, Reykjavik, Iceland.
- Kolb, E., Tanaka, K., 2001. Geologic history of the polar regions of Mars based on Mars Global Surveyor data II. Amazonian period. *Icarus* 154, 22–39.
- Kolb, E., Tanaka, K., 2003. Detailed geologic analysis of part of the south polar layered deposits, Planume Australe, Mars. In: 3rd Mars Polar Meeting.
- Koutnik, M., Byrne, S., Murray, B., 2002. South polar layered deposits of Mars: the cratering record. *J. Geophys. Res.* 107 (E11), 5100–5112.
- Koutnik, M., Murray, B., Byrne, S., 2003. Surface features of the south polar layered deposits and possible terrestrial analogues. In: 3rd Mars Polar Meeting.
- Murray, B.C., Soderblom, L.A., Cutts, J.A., Sharp, R.P., Milton, D.J., Leighton, R.B., 1972. Geological framework of the south polar region of Mars. *Icarus* 17, 328–345.
- Murray, B., Plaut, J., Marsden, P., Schaller, E., Byrne, S., Koutnik, M., 2003. Recent Mars polar resurfacing event suggested by small impact cratering record. In: American Geophysical Union Fall Meeting 2003.
- Mischna, M.M., Richardson, M.I., Wilson, R.J., McCleese, D.J., 2003. On the orbital forcing of martian water and CO₂ cycles: a general circulation model study with simplified volatile schemes. *J. Geophys. Res.* 108, 5062.
- Neumann, G.A., Rowlands, D.D., Lemoine, F.G., Smith, D.E., Zuber, M.T., 2001. The crossover analysis of MOLA altimetric data. *J. Geophys. Res.* 106, 23753–23768.
- Piqueux, S., Byrne, S., Richardson, M.I., 2003. Sublimation of Mars's southern seasonal CO₂ ice cap and the formation of spiders. *J. Geophys. Res.* 108, 5084.
- Plaut, J.J., Kahn, R., Guinness, E.A., Arvidson, R.E., 1988. Accumulation of sedimentary debris in the south polar region of Mars and implications for climate history. *Icarus* 75, 357–377.
- Saunders, R.S., Blewett, D.T., 1987. Mars north polar dunes: possible formation from low-density sedimentary aggregates. *Astron. Vestn.* 21, 181–188.
- Schaller, E.L., Murray, B.C., Rasmussen, J., Byrne, S., 2003. Secondary crater populations on the martian south polar layered deposits. In: American Geophysical Union Fall Meeting 2003.
- Squyres, S., 1979. The evolution of dust deposits in the martian north polar region. *Icarus* 40, 244–261.
- Thomas, P.C., Gierasch, P., Sullivan, R., Miller, D.S., Alvarez del Castillo, E., Cantor, B., Mellon, M.T., 2003. Mesoscale linear streaks on Mars: environments of dust entrainment. *Icarus* 162, 242–258.
- Thomas, P., Squyres, S., Herkenhoff, K., Howard, A., Murray, B.C., 1992. Polar deposits of Mars. In: Kieffer, H.H., Jakosky, B.M., Snyder, C.W., Matthews, M.S. (Eds.), *Mars*. Univ. of Arizona Press, Tucson, pp. 767–795.
- Titus, T.N., Kieffer, H.H., Christensen, P.R., 2003. Exposed water ice discovered near the south pole of Mars. *Science* 299, 1048–1051.
- Toigo, A.D., Richardson, M.I., 2002. A mesoscale model for the martian atmosphere. *J. Geophys. Res.* 107, 5049.
- Toigo, A.D., Richardson, M.I., Wilson, R.J., Wang, H., Ingersoll, A.P., 2002. A first look at dust lifting and dust storms near the south pole of Mars with a mesoscale model. *J. Geophys. Res.* 107, 5050.
- Toon, O.B., Pollack, J.B., Ward, W., Burns, J.A., Bilshi, K., 1980. The astronomical theory of climate change on Mars. *Icarus* 44, 552–607.
- Vasavada, A.R., Williams, J.P., Paige, D.A., Herkenhoff, K.E., Bridges, N.T., Greeley, R., Murray, B.C., Bass, D.S., McBride, K.S., 2000. Surface properties of Mars' polar layered deposits and polar landing sites. *J. Geophys. Res.* 105, 6961–6969.